

Outline of climate and oceanic conditions in the Indian Ocean: an update to mid-2021

Francis MARSAC¹
IRD
UMR MARBEC, Seychelles Fishing Authority
Mahé, Seychelles

Abstract

We examine several descriptors of the ocean status to depict the inter-annual variability and to track trends in the large pelagic ecosystem. The most recent El Niño event occurred from January to July 2019. This was a weak event followed by a positive Indian Ocean dipole from July 2019 to January 2020. The ocean response was a 50-80 m deepening of the thermocline in the West Indian Ocean (WIO) and a shoaling of the thermocline of 20 to 60 m above normal in the East Indian Ocean (EIO). From October 2019 to February 2020, the surface chlorophyll concentration decreased from 30 to 60% below normal in the West Indian Ocean and increased from 40 to 200% above normal in the EIO. On the opposite, a La Niña event developed from August 2020 to March 2021, followed by a short negative Indian Ocean dipole in June-July 2021. Over the whole Indian Ocean basin, after 8 years of a low productivity regime (2007-2014), a shift towards positive anomalies of ocean productivity occurred from 2015 on. In 2019-2020, the productivity was back to low levels (-5 to -11%) in the WIO, whilst it remained 5 to 10% above the mean in the rest of the equatorial basin. Trends in dissolved oxygen concentrations (DOC) are also analysed for 1993-2019 in four large regions. The DOC declining trend in the West and East Indian Ocean could have produced a vertical compression in the optimal habitat for skipjack and yellowfin tuna, notably from 2017 to 2019, thus potentially increasing the vulnerability of these species to the surface gears.

1- Data sources

Various sources of data are used in this study:

- climatic indices. The first category is using sea level pressure data. This includes the Southern Oscillation Index (SOI) that depicts the ENSO cycle, and the Indian Ocean Oscillation Index (IOI, Marsac & Le Blanc, 1998). The second category is based on sea surface temperature-derived, with the Dipole Mode Index (DMI, Saji et al, 1999) reflecting a mode of variability that is specific to the Indian Ocean (and sometimes coupled to the ENSO). The monthly DMI series used here was generated by the Hadley Centre, UK (HadISST1.1 product)
- Sea surface chlorophyll-a (SSC) concentration from SeaWifs (1997-2002) and Modis (2003-present) satellite-mounted sensors, giving an index of ocean surface productivity (enhancement or depletion).
- sea surface temperature from the OISSTv2 dataset (*NOAA_OI_SST_V2 data provided by the NOAA/OAR/ESRL PSD, Boulder, Colorado, USA, <https://www.esrl.noaa.gov/psd/>*) available by month since November 1981 at a spatial resolution of 1°latitude-longitude (Reynolds et al, 2002). Anomalies are based on a 30-year climatology (1981-2010).
- NOAA/NCEP Global Ocean Data Assimilation System (GODAS) providing monthly fields of temperature, salinity, vertical velocity and current for 40 depth levels (5 to 4500 m), along a 1° longitude/0.33° latitude grid globally. Here, we use the model product to derive the depth of thermocline by interpolating the 20°C isothermal depth between consecutive depth levels in the upper 300 m of the water column.

¹ Email : francis.marsac@ird.fr

- Copernicus Marine Service products (<https://marine.copernicus.eu/>). The Copernicus catalogue includes a wide range of ocean models of global coverage with high time and space resolutions (hour-day-month; 2 to 25 km) for physical and biogeochemical variables, including hindcasts, nowcasts and forecasts. In this paper, we use the oxygen concentration data from a global ocean biogeochemistry hindcast (*product code: global_reanalysis_bio_001_029*), a data-assimilated model for 1993 to 2019, on 75 vertical levels, by month, at a 0.25 degree spatial resolution.

Datasets and methods used to produce the variables are detailed in Marsac (2013). The most recent data incorporated in this analysis is from August 2021. Other shorter data series include data until November 2019 or February 2021.

2- Variability and trends in the oceanic environment

2.1 Climatic indices

The **SOI** indicates that the last El Niño event recorded (negative SOI index) occurred from January to July 2019. This weak El Niño peaked from April to June 2019 (Fig. 1a). The most recent anomaly was a La Niña event (positive SOI index) which spanned 8 months, from August 2020 to March 2021. Before and after this Niña event, the ENSO conditions were neutral.

An ensemble analysis of multiple models predicts a transition from the present ENSO-neutral conditions to La Niña conditions by October 2021, with a 70-80% chance of La Niña during prevailing through the 2021-2022 Northern hemisphere winter (Fig. 2) (NOAA, 2021).

The **IOI** was dominated by negative values (reflecting low-pressure anomalies and warm conditions in the West IO) over several years, from 2007 through 2015 (Fig. 1b). The 2014-15 negative IOI event was synchronous with El Niño. Another negative IOI episode developed from February 2019 to mid-2020, with a stronger magnitude than in 2014-15. The corresponding SOI values were negative but did not reach the threshold required to qualify as El Niño. By contrast, a strong positive IOI developed for almost 12 months through the second semester of 2016 and first quarter of 2017 when SOI values were slightly positive (but still remaining in the neutral-like mode). Eventually, another positive IOI was observed during the first quarter of 2021, in synchrony with the 2020-21 La Niña event (Fig. 1b)

The **DMI** has shown mostly positive values since 2006, whereas alternating oscillations between negative and positive episodes occurred in the period 1970-2005 (Fig. 3). The positive DMIs for the past 15 years likely denotes a gradually warming West Indian Ocean. In June-July 2021, the Australian Bureau of Meteorology evidenced low DMI values (on a weekly basis) suggesting a weak negative dipole was underway. The strongest climatic perturbations occur when positive dipoles arise in coincidence with El Niño, and negative dipoles with La Niña. The positive IOD/El Niño synchrony may cause droughts in the Eastern Indian Ocean (EIO) and severe rainfall anomalies in the Western Indian Ocean (WIO). An opposite response arises with the negative IOD/La Niña synchrony.

An ensemble analysis of several models predicts neutral conditions for the Indian Ocean Dipole to persist until January 2022 (> 80% probability), then gradually increasing values towards the positive IOD threshold from February 2022 on (Australian Bureau of Meteorology, 2021) (Fig. 4).

We further analysed the SST anomalies in the two area boxes used to compute the DMI: WIO (50°E-70°E / 10°N-10°S) and EIO (90°E-110°S / 0°-10°S) in the period 2015-2021 (Fig. 5). Firstly, the SST fluctuations in the WIO essentially concerned positive anomalies, while the SST fluctuations in the EIO ranged from positive (+1.2°C) to negative anomalies (-1.5°C). Secondly, among the two major warm episodes recorded in the WIO, in 2015/16 and 2019/20, only the latter was conducive to a positive dipole, as the corresponding SST in the EIO was strongly negative (-1.5°C anomaly).

All three indices are significantly correlated, with the highest correlation found between IOI and SOI ($r_s = +0.47$, $p < .001$). The DMI is more correlated with IOI ($r_s = -0.41$, $p < 0.001$) than with SOI ($r_s = -0.20$, $p < 0.001$). The fact that DMI and IOI both depict a mode of variability which is specific to the Indian Ocean is a good reason for such a higher correlation.

2.2 Main oceanic features over 2019-2021

Maps of anomalies for SST, the 20°C isothermal depth and SSC are presented in Fig. 6 (a - d).

- The SST signature denoting the start of a positive dipole appeared in July 2019, with cold anomalies gradually developing along the South of Java and the West of Sumatra (-1° to -3°C). Positive SST anomalies ($+1^{\circ}$ to $+2^{\circ}\text{C}$) appeared in the West Indian Ocean in October 2019. The largest contrast between cold anomalies in the East and warm anomalies in the West was reached in November 2019. The dipole-related SST pattern vanished in January 2020.
- Deep anomalies of the mixed layer depth (Z20a) in the central and western Indian Ocean are associated to positive dipole events. Such anomalies appeared in October 2019, which is 2 months after the onset of SST anomalies in the East Indian Ocean. The deep thermocline anomaly propagated to West while intensifying. A well-developed dipole pattern then was in place in December 2019, characterized by the shoaling of the thermocline in the East Indian Ocean by 20 to 60 m above normal, and a deepening in the West Indian Ocean to about 50 to 80 m below normal. The phenomenon then started to decrease in January but a deep thermocline signature (30 m deeper than normal) was still clearly visible until June 2020, thus six months after the disappearance of the dipole-related SST pattern.
- The 2019 positive dipole also affected the ocean productivity. There was an elevated chlorophyll (Chl) concentration (ranging from +40% to 200% of the average Chl concentration) along the coasts of Java and Sumatra in synchrony with the cold SST anomalies. In the West Indian Ocean, the Chl concentration was reduced by -30% in October-November. This reduction reached -60% along the East African coast in January-February 2020. Therefore, a Chlorophyll dipole pattern was clearly observable from October 2019 to February 2020. Very high levels of Chl were also noticeable in the Arabian Sea from January to March 2020.
- In January-February 2021, a negative dipole-like pattern was observable in the thermocline depth, with deep thermocline in the East Indian Ocean and shallow thermocline in the West. However, this situation does not reflect a negative dipole event at that date, as the Australian Bureau of Meteorology diagnosed a negative dipole for June-July 2021 only.

3- Inter-annual variability and trends of primary productivity in four ecoregions of the Indian Ocean

The same four large ecoregions that were initially presented by Marsac & Demarcq (2019) were used here. These ecoregions are a simplified version of those defined at the 1st Ecoregion workshop of the IOTC organized in 2019. We consider two ecoregions (MONW in the West, MONE in the East, separated at 77°E) within the large MONS Longhurst province (Longhurst, 1998). Our MONW ecoregion also encompasses the Somalian part of the Longhurst's ARAB province. We also delineate an ecoregion for the Mozambique Channel (MOZ) corresponding to the northern region of the Longhurst's EAFR province but excluding the east coast of Madagascar. Finally the 4th ecoregion matches the almost entire Longhurst's ISSG province. The four ecoregions (Fig. 7) are assigned in the following boundaries:

- MONW : $40^{\circ}\text{E} - 77^{\circ}\text{E} / 10^{\circ}\text{N} - 12^{\circ}\text{S}$
- MONE : $77^{\circ}\text{E} - 120^{\circ}\text{E} / 10^{\circ}\text{N} - 12^{\circ}\text{S}$ (excluding regions extending east of Sumatra and north of Java)
- MOZ : $30^{\circ}\text{E} - 47^{\circ}\text{E} / 12^{\circ}\text{S} - 30^{\circ}\text{S}$
- ISSG : $47^{\circ}\text{E} - 120^{\circ}\text{E} / 12^{\circ}\text{S} - 30^{\circ}\text{S}$

In order to compare the overall productivity of each ecoregion, we computed the SSC annual average as displayed in Fig. 8. The MOZ region is the most productive one, MONW ranks second, MONE ranks third and the less productive region is the ISSG.

MOZ SSC concentration (annual average) ranged from 0.35 to 0.43 mg.m^{-3} with two periods of higher productivity: 1998 to 2002 (mean=0.42 mg.m^{-3}), 2015-2020 (mean=0.41 mg.m^{-3}) separated by 12 years or relatively lower productivity. The lowest SSC value was observed in 1997 when a strong El Niño and positive dipole was developing. The mesoscale vertical dynamics caused by eddies propagating through the Mozambique Channel and the chlorophyll-rich waters of the Mozambican and western Madagascar

shelves, transported offshore by the action of eddies, contribute to generate an average enhanced productivity in this region.

MONW SSC concentration ranged from 0.15 to 0.22 mg.m⁻³ with a sustained high productivity during 6 years, from 2000 to 2005 (mean=0.21 mg.m⁻³) and again in 2016-2017 (mean=0.20 mg.m⁻³). Likewise MOZ, the lowest recorded SSC value was in 1997.

By contrast to the two previous Western IO provinces, an anomalously high SSC concentration was recorded in MONE, in 1997 (0.37 mg.m⁻³), when the coupled Niño/IOD+ event boosted the production in the eastern edge of the Indian Ocean. The SSC in MONE exhibited an overall decrease until 2014 (from 0.25 to 0.19 mg.m⁻³). An upward trend has been observed since then, with a maximum value of 0.25 mg.m⁻³ in 2019, in relation to the positive dipole event mentioned earlier.

Finally, SSC in ISSG fluctuated in a short range, between 0.09 and 0.13 mg.m⁻³ denoting oligotrophic conditions. Slightly higher concentration was observed in 2000 and during the last 4 years of the series.

The series were normalized to perform a direct comparison of inter-annual changes across ecoregions. The normalization consists in calculating the deviation (in %) of each year to the pluri-annual mean, in each region. The normalized series (Fig. 9) exhibit several features:

- The two western ecoregions (MONW and MOZ) were negatively affected by the 1997 coupled Niño/IOD+ event with 17% and 11% reduction in SSC concentration, respectively; whereas a 69% increase of SSC occurred in the eastern region (MONE). By contrast, the 1997 coupled Niño/IOD+ event did not cause any particular signal in ISSG, as the strongest anomalies propagate north of 10°S;
- A phase with positive SSC anomalies prevailed in ISSG, MOZ and MONW from 1998 to 2006, but with a time shift across ecoregions. The first SSC positive anomaly occurred in ISSG (+17% in 2000), then MOZ (+9.6% in 2002) and finally MONW (+18.3% in 2004). This phase spanned 6 years in MONW.
- During 1997-2005, the SSC in MONE had a declining trend in SSC, as opposed to the other ecoregions. In 2006, the development of an El Niño/positive IOD event boosted the productivity in the East, and caused a decline in productivity in the West a few months later (2007).
- From 2007 on, all four ecoregions went through the same pattern, i.e. a low productivity from 2007 to 2014 (reaching a maximum of -20% reduction), and a shift to positive productivity (up to 10% increase) from 2015 to 2018. In 2019, only MONW showed a strong decline in productivity, in relation to the positive dipole event. In that ecoregion, 2020 remains lower than normal, whereas the three other ecoregions showed enhanced productivity of 6 to 11% above the mean.

4- Dissolved oxygen trends

The dissolved oxygen concentration (DOC) was analysed on a monthly basis, from 1993 to 2019, in four large regions that overlap partly with the ecoregions described earlier. The West Indian Ocean (WIO, 50E-70E/10S-5N) is included in MONW, the East Indian Ocean (EIO, 80E-105E/10S-5N) is part of the MONE, and the South Subtropical Gyre (SSG, 50E-110E/30S-15S) is included in the ISSG. Only the Arabian Sea (50E-70E/5N-25N) is a new area in our analysis. The limits of these large regions is based on the main features of the spatial pattern of dissolved oxygen in the Indian Ocean (not shown). As the dissolved oxygen saturation in the water depends on the temperature, we also plot the sea surface temperature (SST) trend on the graphs. Indeed, SST is not the main driver of oxygen saturation at depth; however, it provides some indication with regard to the overall trend in relation to global warming.

4.1 Biogeochemical model hindcast analyses by large areas

In the Arabian Sea (Fig 10a), the DOC at 100 m increased by 35% from 1993 to until 2016, then decreased by 14% during the last 3 years of the series. Over the whole series studied, the minimum and maximum DOC values were 1.8 and 2.5 ml L⁻¹. The DOC at 200 m fluctuated without any trend, but declined sharply by 27% in the last 3 years of the series. The DOC values ranged between 0.30 and 0.45 ml L⁻¹. SST has been steadily increasing on an average of 0.082°C per decade.

In the WIO, the DOC at 100 m fluctuated without trend until 2016, and then declined by 8% during the last 3 years of the series. In 2019, the DOC fell below 2.5 ml L⁻¹. By contrast, at 200 m, the DOC showed a gradual decline of 0.1 ml L⁻¹ per decade. The maximum DOC was 1.92 ml L⁻¹ (in 1993) and 1.46 ml L⁻¹ (in 2019). During the same period, SST showed a steadily increasing trend of 0.125°C per decade.

In the EIO, similarly to the WIO, the DOC at 100 m fluctuated without trend until 2016, and then decreased by 30% from 2016 to 2019, to reach a lowest 1.5 ml L⁻¹. The whole DOC series at 100 m stayed below 2.5 ml L⁻¹. The DOC at 200 m decreased gradually over the study period, from 1.19 to 0.80 ml L⁻¹. SST showed an increasing trend of 0.096°C per decade.

In the SSG, the DOC at 100 m exhibited an overall declining trend of 0.027 ml L⁻¹ per decade (1.8% reduction). DOC values ranged between 3.74 and 3.86 ml L⁻¹ that are levels well above the range recorded in the three other studied regions. At 200 m, the DOC showed a dramatic decline of 0.142 ml L⁻¹ per decade (8% decline) between 1993 and 2012. Then the trend reversed and the DOC slightly increased from 2012 on at a rate of 0.07 ml L⁻¹ per decade (over 7 years). The SST trend has been highly positive, at a rate of 0.224°C per decade, the largest among all regions studied here.

4.2 Discussion

The dissolved oxygen is a key biogeochemical parameters as oxygen gradients condition the vertical and horizontal distributions of organisms. There are concerns about the expansion of the Oxygen Minimum Zones (OMZ), found between 300 to 700 m, since the 1960s in relation to climate change. Shoaling of the upper boundaries of the OMZ is an ongoing process, which can affect all marine organisms via direct or indirect mechanisms (Stramma et al, 2008; Gilly et al, 2013). OMZs are generally associated with eastern boundary current systems, but the OMZs in the Indian Ocean are located in the north of the basin (Arabian Sea and Bay of Bengal). A stagnant circulation reducing the supply of oxygen in the deep layers and detritus falling from the highly productive waters above and rapidly depleting oxygen below sustain these IO OMZs.

Over the period 1993-2019, the Copernicus biogeochemical reanalyses show clear declines in DOC at 200 m in the two equatorial regions (WIO and EIO) and the subtropical regions (SSG). Such declines occurred as the ocean temperature is trending upwards. Although the processes leading to (or sustaining) low dissolved oxygen levels in the ocean are complex (including low ventilation, remineralization of sinking detritus) and play in interaction, climate models indicate global warming as the primary cause of ongoing deoxygenation. The decreasing solubility of oxygen is estimated to account for >50% of the oxygen loss in the upper 1000 m of the ocean (Schmidtke et al, 2017). The Arabian Sea exhibits a different DOC trend compared to the other regions studied here. Although temperature has also been increasing in that region, the DOC has not changed substantially at 200 m, and the DOC at 100 m has even been increasing. Stramma et al (2008) already mentioned the absence of substantial change in the north Indian Ocean OMZ. The increase of DOC at 100 m in the Arabian Sea is quite difficult to interpret. Possible changes in the wind pattern, due to a weakening of the Walker circulation, would induce easterlies anomalies with a deepening of the thermocline in the central Arabian Sea, accumulating more oxygenated water in the upper layer.

Tunas are among the pelagic fish species that are largely constrained by oxygen supply in the water column because of their high metabolic requirements. Tropical tunas spend most of their time in the well-oxygenated waters of the mixed layer. Skipjack is the least tolerant species within the group of major tunas. When DOC falls below 4 mg L⁻¹, skipjack increase their swimming speed (to enhance oxygen uptake). Yellowfin responds in the same way for concentrations below 2.5 mg L⁻¹ (Dizon, 1977). By contrast, bigeye have a greater tolerance to low O₂ levels (often found in ambient DOC below 1.9 mg L⁻¹) which explains their extensive diel vertical movements. Lethal DOC levels are at 2.45, 1.49 and 0.52 ml L⁻¹ for skipjack, yellowfin and bigeye, respectively (in Lehodey et al, 2011). From the DOC trends shown in Fig. 10, the optimal vertical habitat (OVH) of skipjack is restricted to the upper 100 m in the regions north of 10°S. As for yellowfin, its OVH does not extend deeper than ~150 m in the Arabian Sea and East Indian Ocean, and can reach 200 m in the West Indian Ocean. Bigeye OVH would only be limited to ~200m in the Arabian Sea, whereas it would extend much deeper in all other regions. In the SSG, there is no DOC limitation in depth for the three tropical species in the upper 1000 m.

The gradual decline in DOC in the West and Eastern Indian Ocean has been causing a habitat compression since 2017, making yellowfin and skipjack more accessible in the upper layer (above 100 m). Potentially, their catchability may have increased for the surface gears during that period.

5- Conclusion

The most recent anomalous climatic event in the Indian Ocean, at interannual scale, is a positive Indian Ocean dipole, which occurred from July 2019 to January 2020. An anomalously deep thermocline persisted until June 2020 in the WIO, six months after the end of the dipole-related SST pattern. This dipole caused a lesser productivity at the base of the food web in the WIO, whilst productivity was anomalously high in the EIO.

Interestingly, an overall below-than-normal productivity was observed in all four ecoregions studied for 8 consecutive years from 2007 to 2014. A shift towards above-than-normal productivity occurred from 2015 on. However, a return to low productivity was recorded in the sole West region (MONW) in 2019 and 2020 whilst the other regions had chlorophyll levels from 5 to 10% above normal.

The oxygen conditions at depth have been on a declining trend in all regions except in the Arabian Sea. Such trend may have caused a habitat compression in the WIO and EIO since 2017, rendering yellowfin and skipjack tunas more concentrated in the upper 100/150 m, and potentially, increasing the vulnerability of these species to surface gears, compared to the previous years.

Acknowledgements

We are grateful to the Climate Centre of the Seychelles Meteorological Authority, and particularly to Beryl Andrade, a quality control technician of this Centre, for the provision of sea level pressure data used to compute the IOI.

References

- Bureau of Meteorology, Australia (2021). Indian Ocean Dipole outlooks. <http://www.bom.gov.au/climate/enso/#tabs=Indian-Ocean>
- Dizon, A.E. (1977) Effect of dissolved oxygen concentrations and salinity on swimming speed of two species of tunas. Fishery Bulletin US, 75, 649–653.
- Gilly, W.F., Beman, J.M., Litvin, S.Y., Robison, B.H. (2013). Oceanographic and biological effects of shoaling of the oxygen minimum zone. *Annual review of Marine Science*, 5: 393-420.
- Longhurst, A. (1998). The ecological geography of the sea. Academic Press.
- Lehodey, P., Hampton, J., Brill, R.W., Nicol, S., et al. (2011) Vulnerability of oceanic fisheries in the tropical Pacific to climate change. In: J.D. Bell, Johnson, J.E. & Hobday, A.J. (Eds) Vulnerability of tropical Pacific Fisheries and Aquaculture to climate change. Secretariat of the Pacific Community, New Caledonia.
- Marsac, F. (2013). Outline of climate and oceanographic conditions in the Indian Ocean: an update to August 2013. *15th Session of the Working Party on Tropical Tuna*. IOTC-2013-WPTT15-09, 14 p.
- Marsac, F., Demarcq, H. (2019). Outline of climate and oceanic conditions in the Indian Ocean: an update to mid-2019. *21st Session of the Working Party on Tropical Tuna*. IOTC–2019–WPTT21–24, 19 p.
- Marsac, F., Le Blanc, J-L. (1998). Interannual and ENSO-associated variability of the coupled ocean-atmosphere system with possible impacts on the yellowfin tuna fisheries of the Indian and Atlantic oceans. In: J.S. Beckett (Ed). *ICCAT Tuna Symposium. Coll. Vol. Sci. Pap.*, L(1) : 345-377.
- NOAA, 2021. Climate Diagnostics Bulletin August 2021. Near real-time ocean/atmosphere, monitoring, assessment and prediction.

Reynolds, R.W., Rayner, N.A., Smith, T.M., Stokes, D.C., and Wang, W. (2002): An improved in situ and satellite SST analysis for climate. *J. Climate*, 15, 1609-1625

Saji, N.H., Goswami, B.N., Vinayachandran, P.N., Yamagata, T. (1999). A dipole mode in the tropical Indian Ocean. *Nature* 401: 360-363

Schmidtko, S., Stramma, L., Visbeck, M. (2017). Decline in global oceanic oxygen content during the past five decades. *Nature* 542, 335–339. doi: 10.1038/nature21399;pmid: 28202958

Stramma, L., Johnson, G.C., Sprintall, J., Mohrholz, V. (2008). Expanding oxygen minimum zones in the tropical oceans. *Science*, 320, 655-658. doi 10.1126/science.1153847

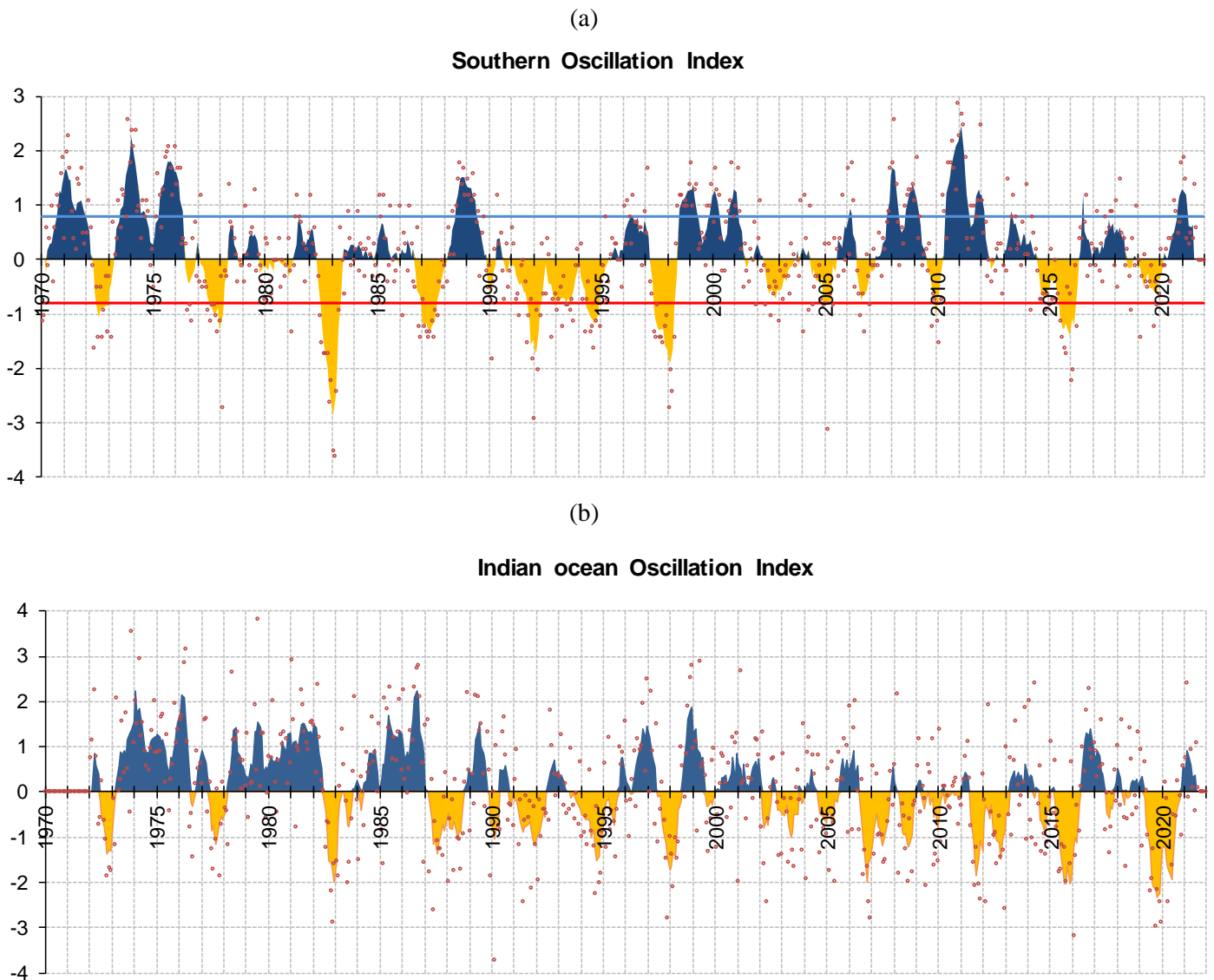


Fig.1 – (a) The Southern Oscillation Index (SOI) and (b) the Indian Oscillation Index (IOI), January 1970 to August 2021. The color shaded area represents the 5-month moving average, whereas observed monthly values are shown in red dots. In the upper panel, El Niño events correspond to the extreme negative values (below the red threshold line) whereas La Niña events are described by the extreme positive values of the SOI (above the blue threshold line).

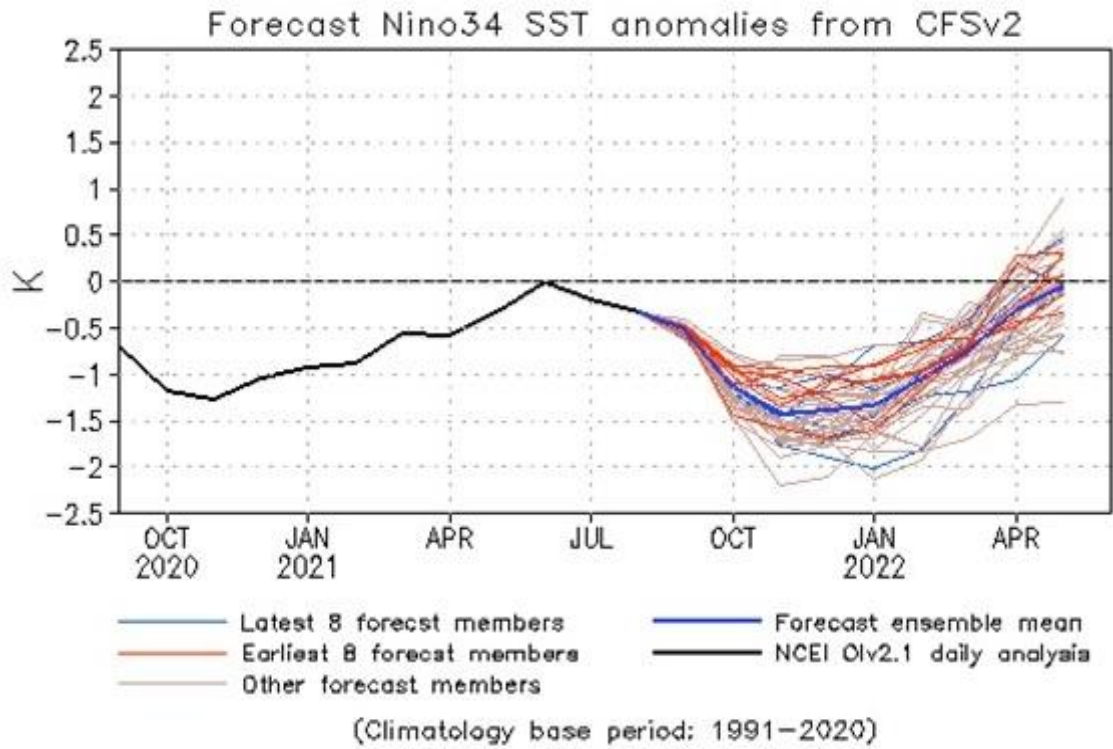


Fig.2 – SST anomalies forecast for Niño 3-4 region (East Pacific ocean) indicating the forecasted trend of the SOI from September-2021 to May 2022 (NOAA, 2021)

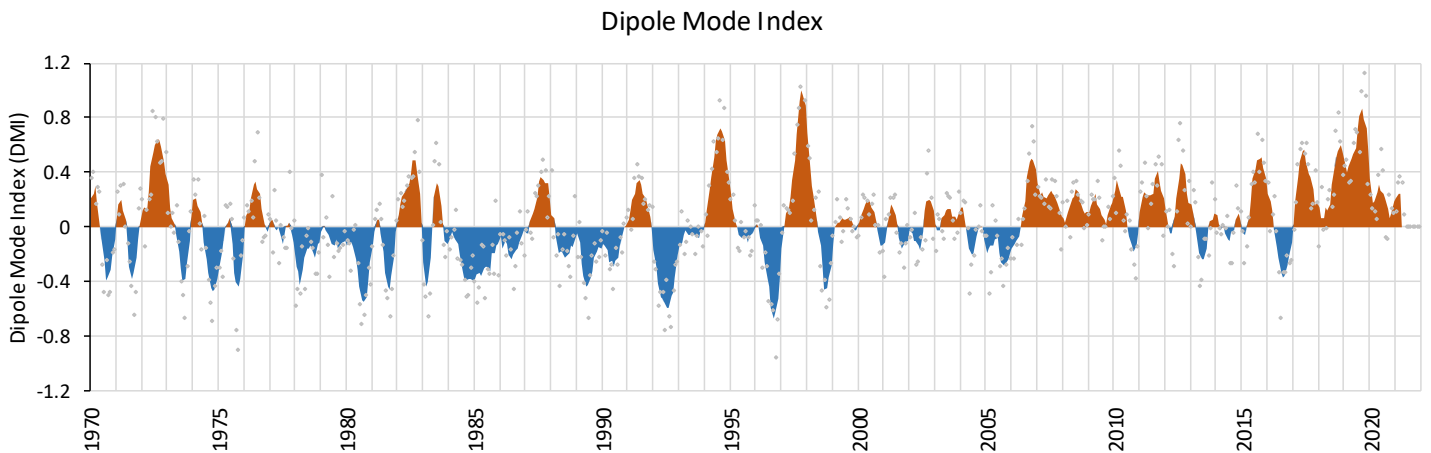


Fig.3 - Dipole mode, January 1970 – May 2021. The shaded area of IOI is a 5-months moving average whereas observed monthly values are represented in black empty dots. The DMI series is 5-month moving average. For a given anomaly, IOI and DMI are frequently in opposite sign. Source: Hadley Centre, UK (HadISST1.1 product).

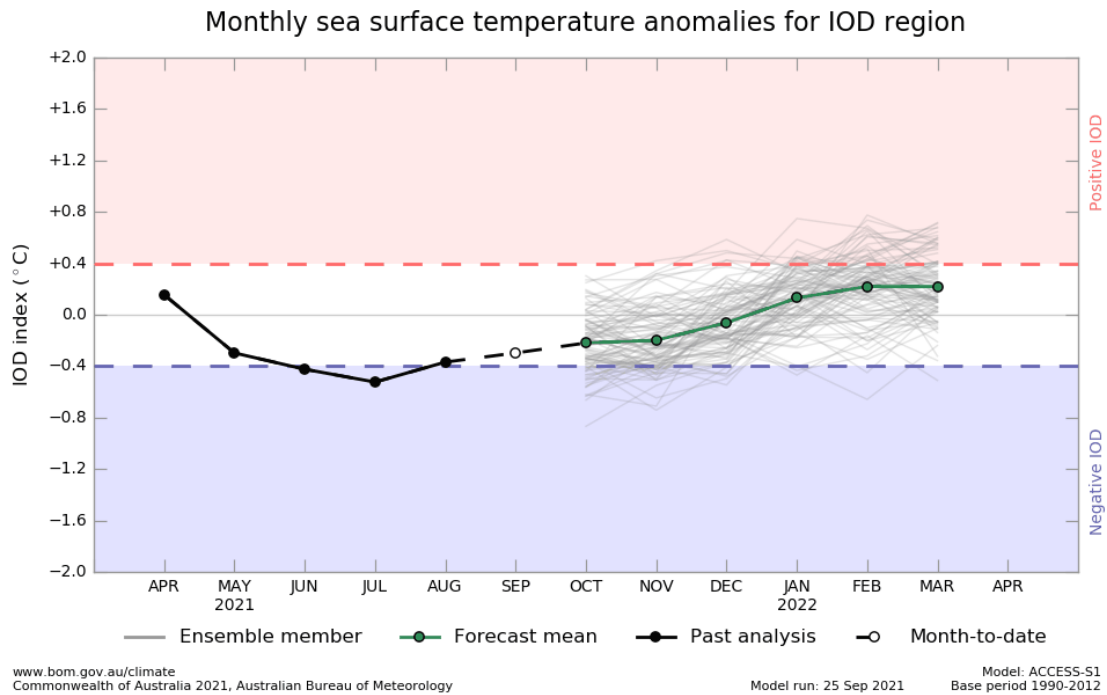


Fig.4 – Dipole mode forecast through predicted monthly sea surface anomalies for the Dipole mode region (Australian Bureau of Meteorology (<http://www.bom.gov.au/climate/enso/#tabs=Indian-Ocean>))

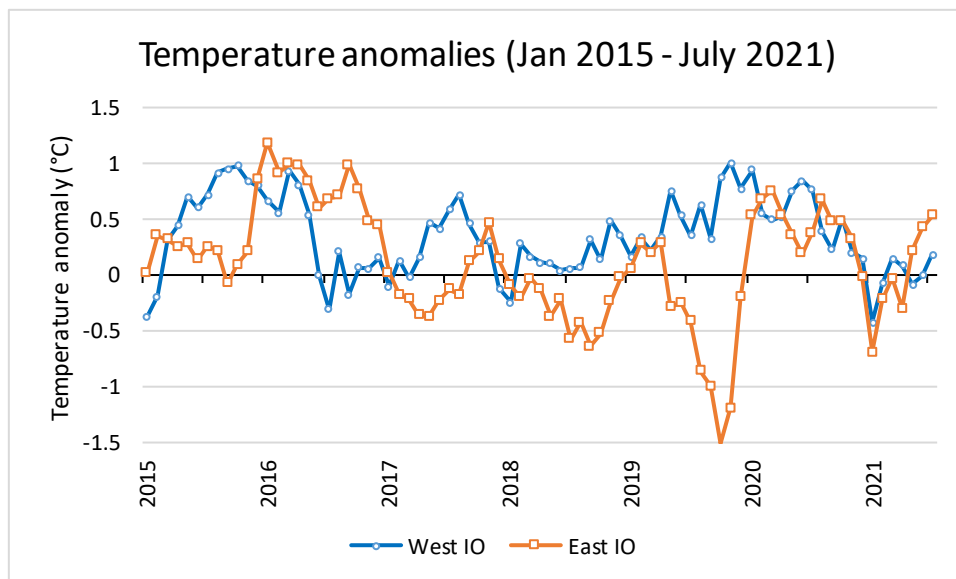


Fig.5 -Monthly SST anomalies in the Western and Eastern area boxes used to compute the DMI, for January 2015 to July 2021. WIO box: 50°E-70°E / 10°N-10°S , EIO box: 90°E-110°E / 0°-10°S (source: OISSTv2)

2019

SSTa

Z20a

Chla

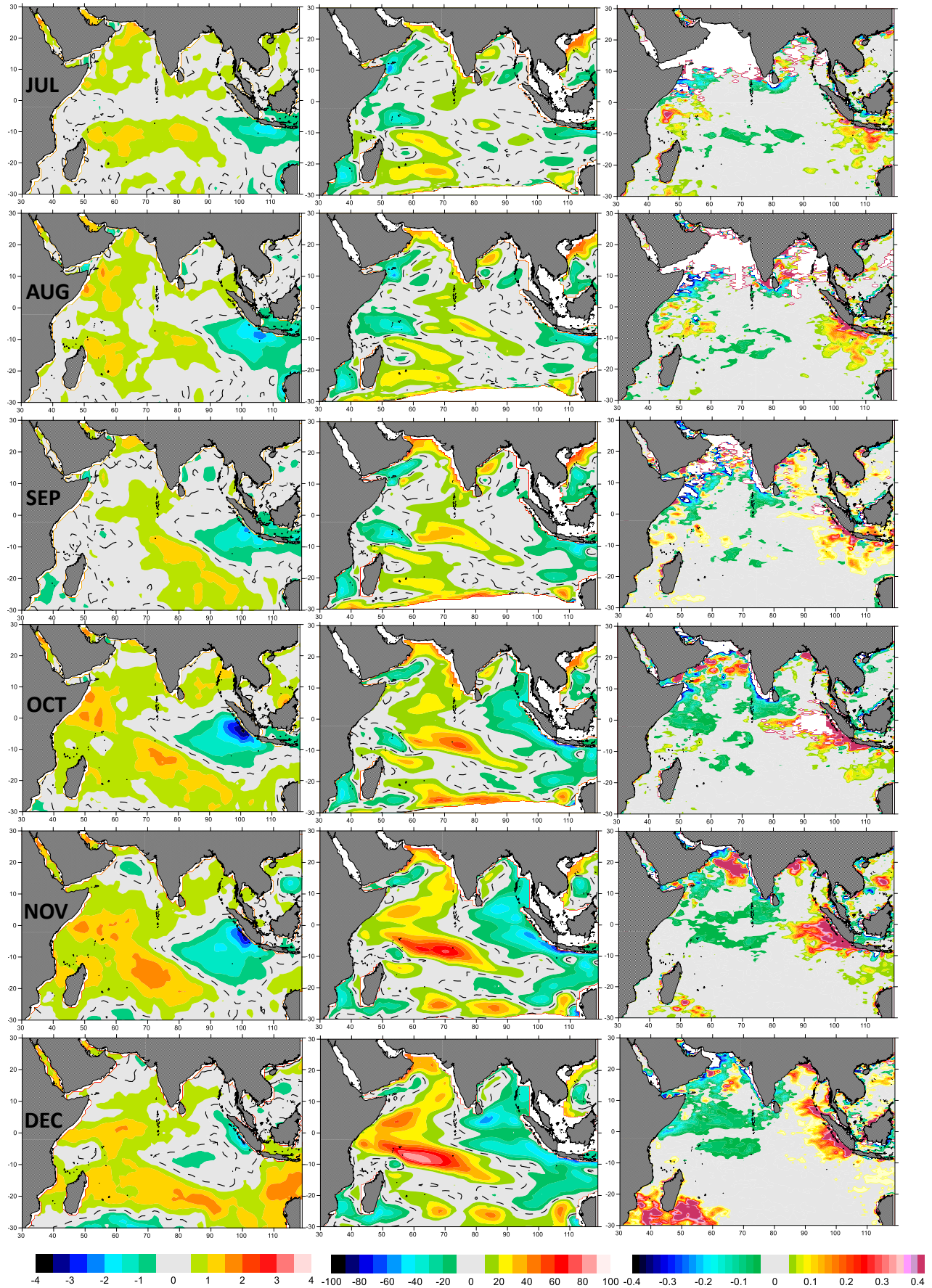


Fig. 6a – Geographic distribution of anomalies for sea surface temperature (°C, left), 20°C isothermal depth (m, middle) and sea surface chlorophyll (mg.m⁻³, right) for the second semester of 2019. Grey shading indicates minor anomalies about the mean. Thus, only the more significant anomalies (colour shading) are highlighted.

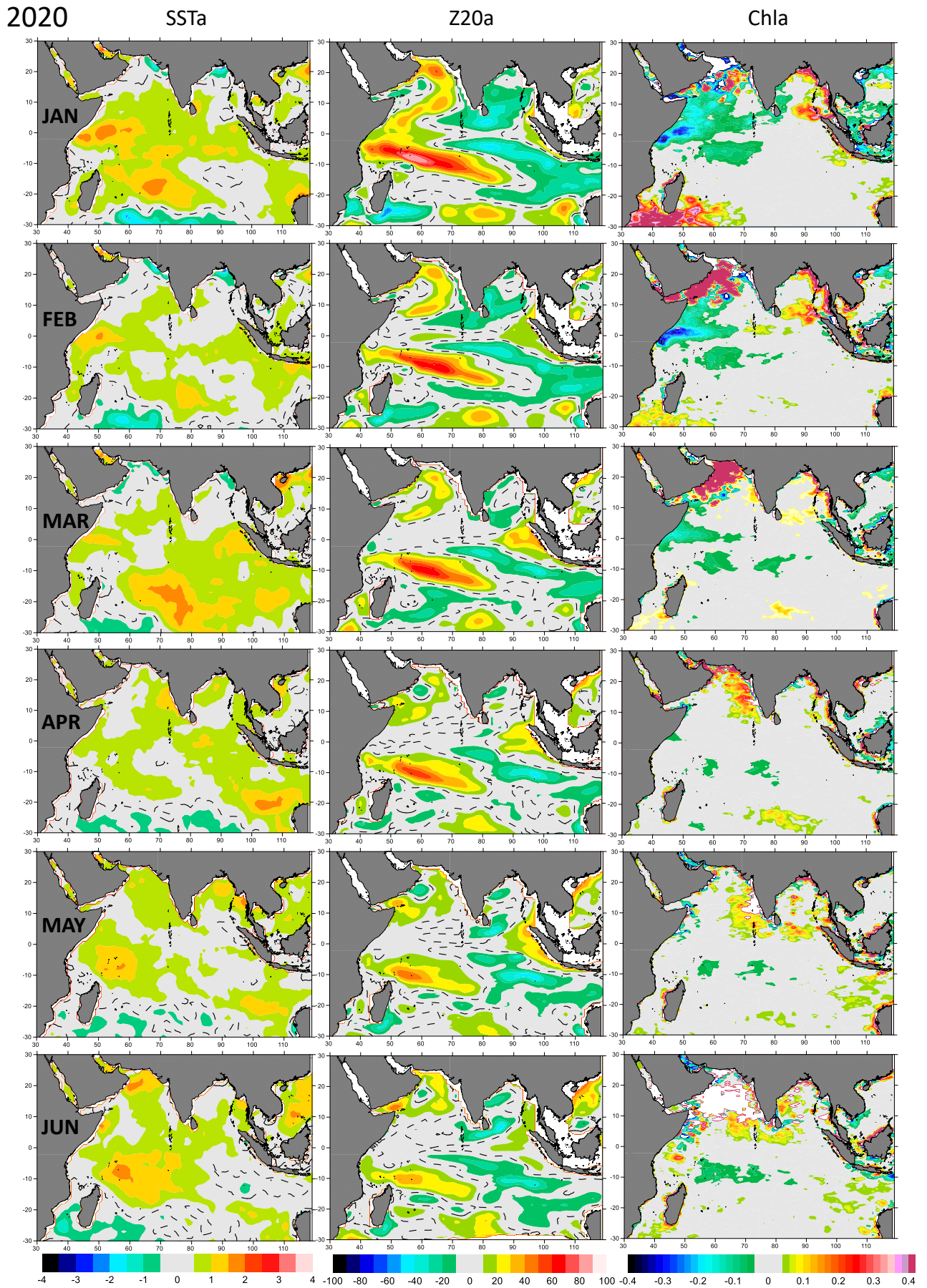


Fig. 6b – Same as above, for the first semester of 2020.

2020

SSTa

Z20a

Chla

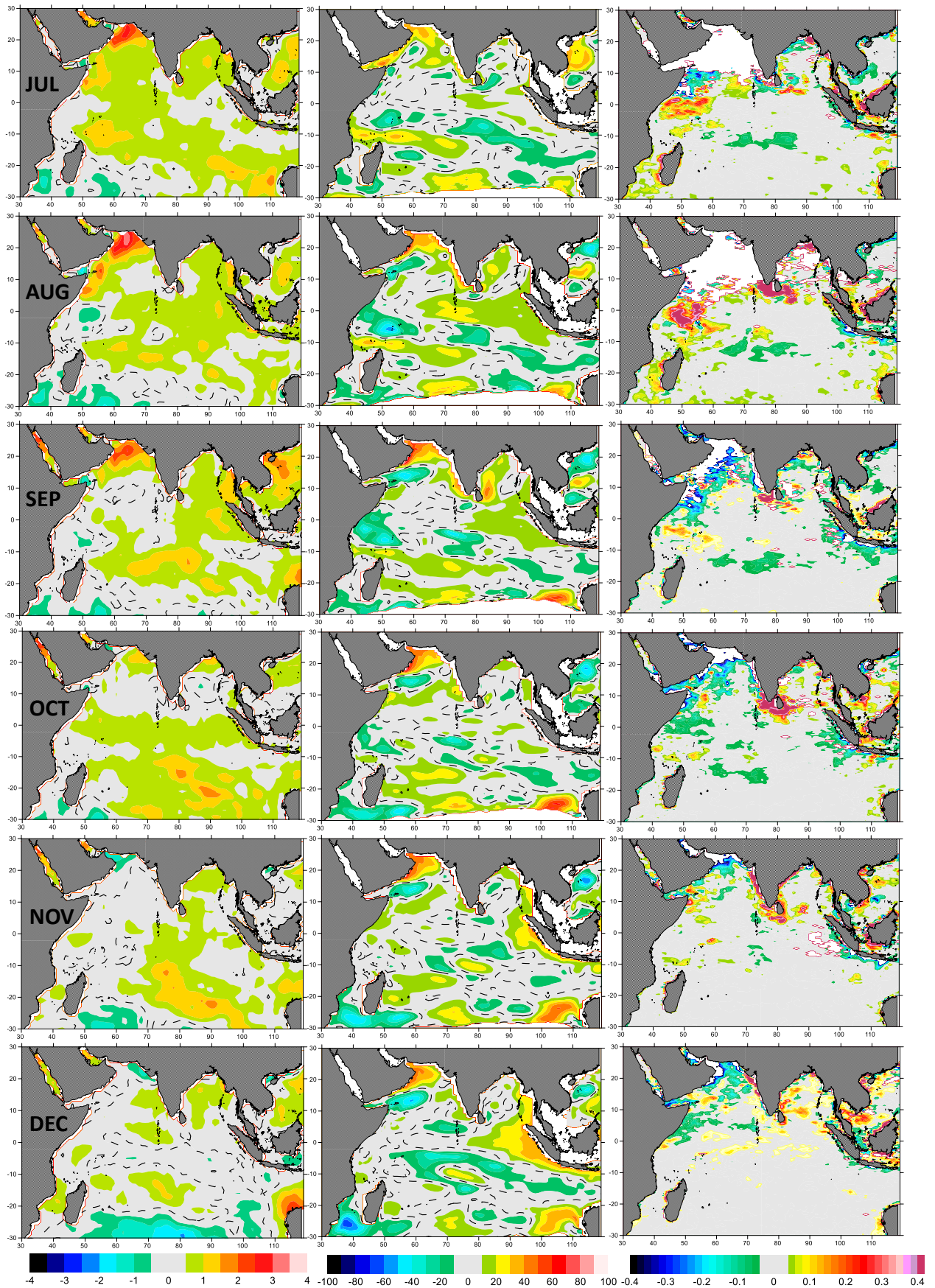


Fig. 6c – Same as above, for the second semester of 2020.

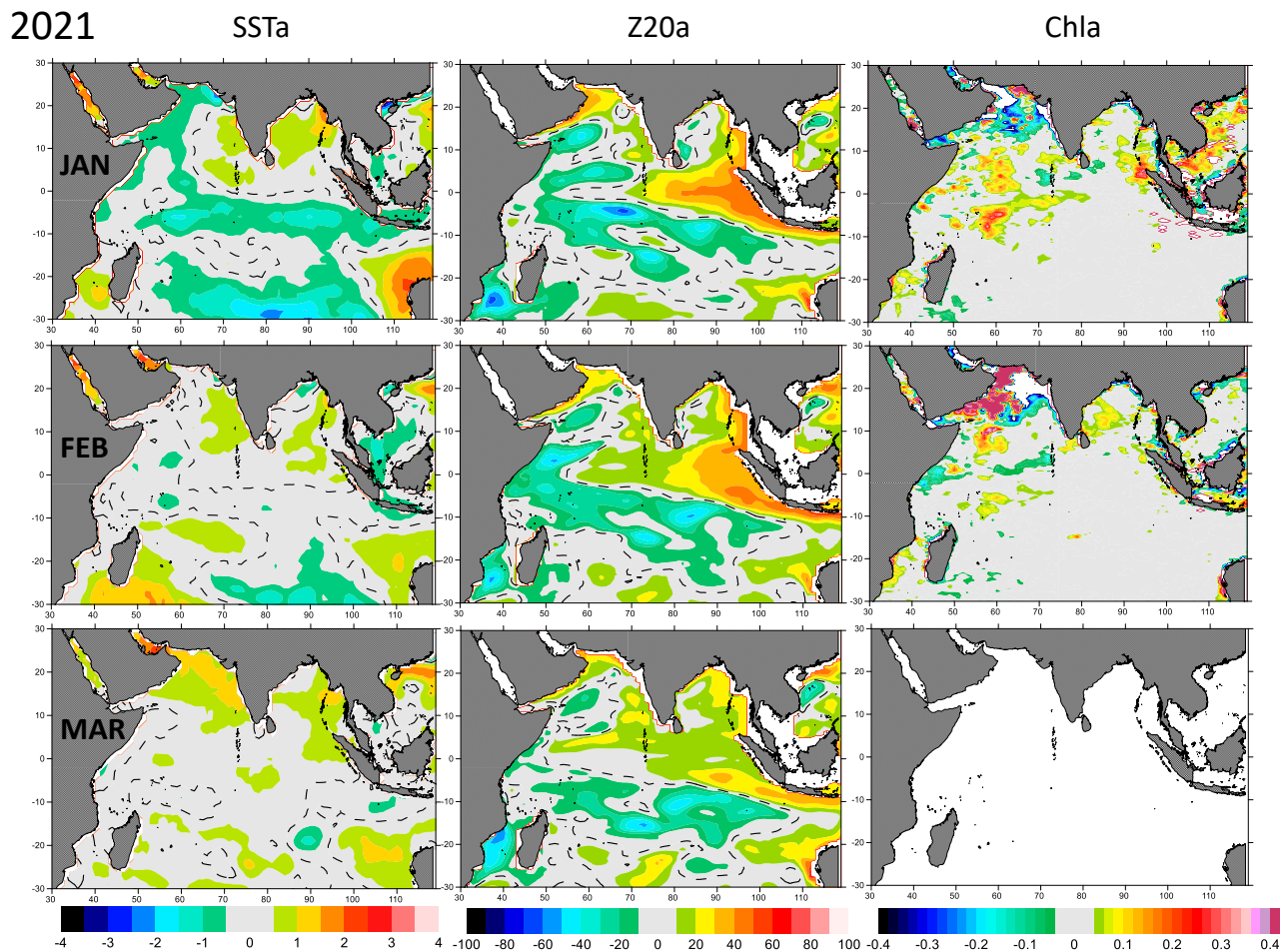


Fig. 6d – Same as above, for the first quarter of 2021

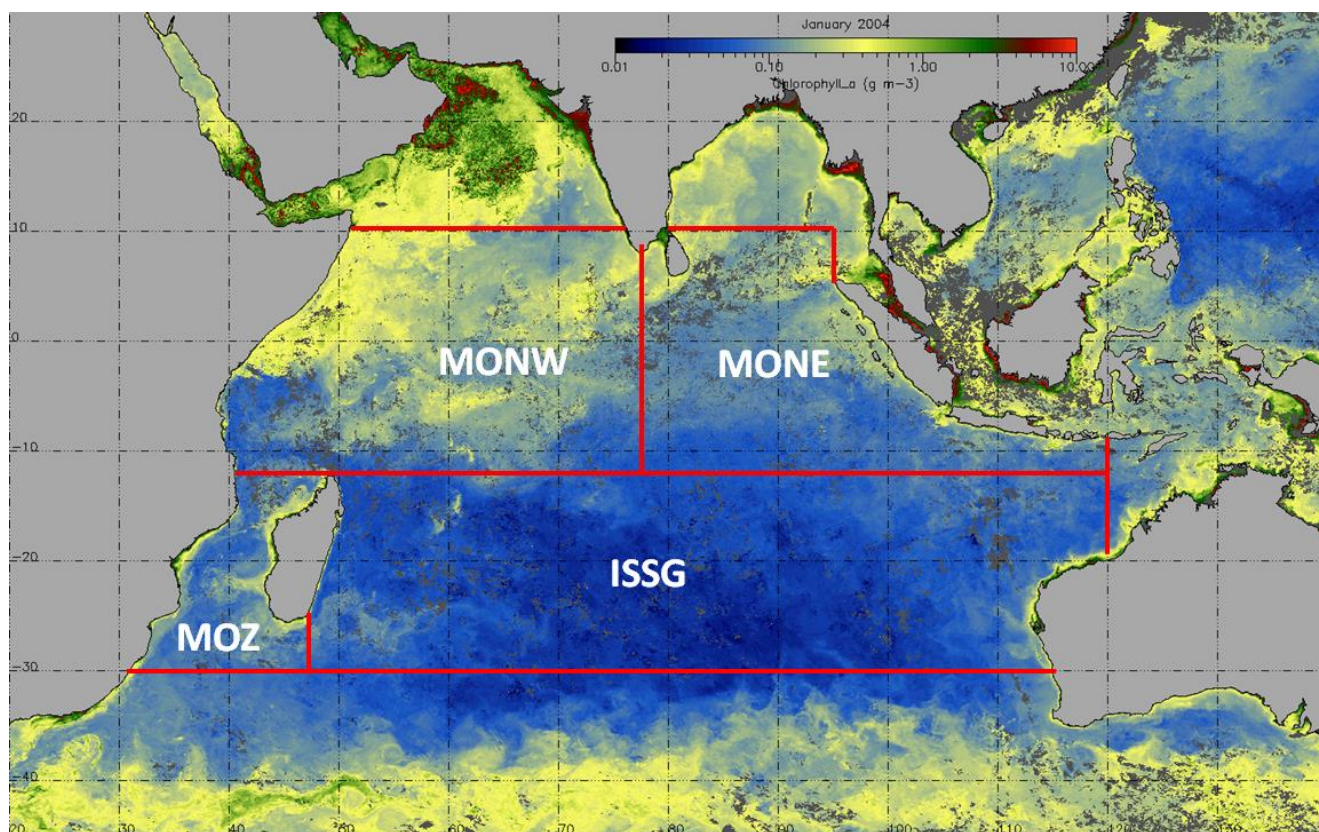


Fig. 7 – Boundaries of the four ecoregions studies in this paper. The background image is the chlorophyll concentration measured by MODIS in January 2004.

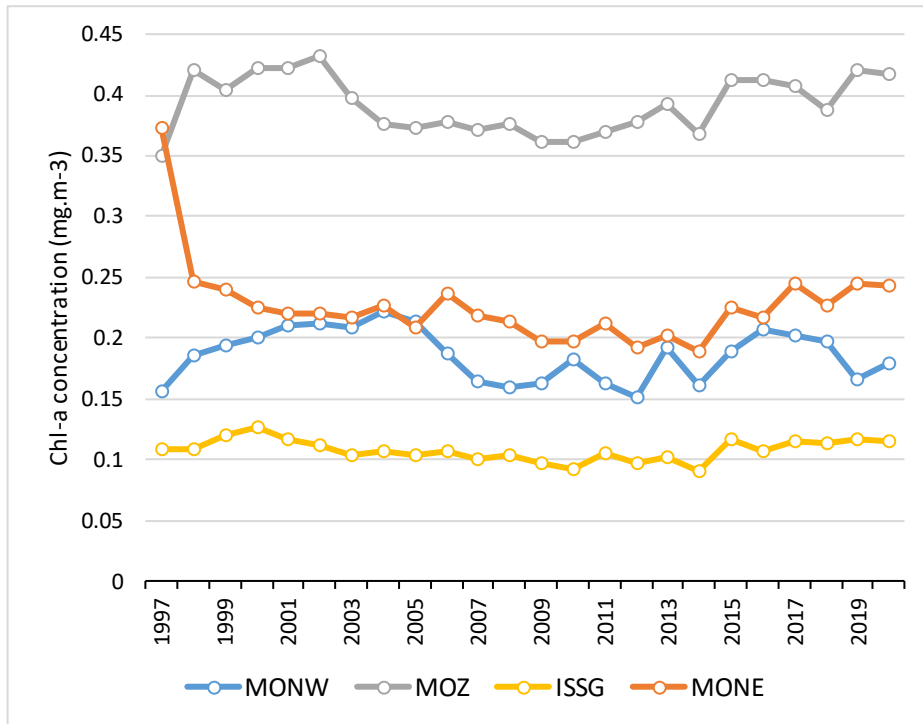


Fig. 8 - Mean annual SSC for each large ecoregion

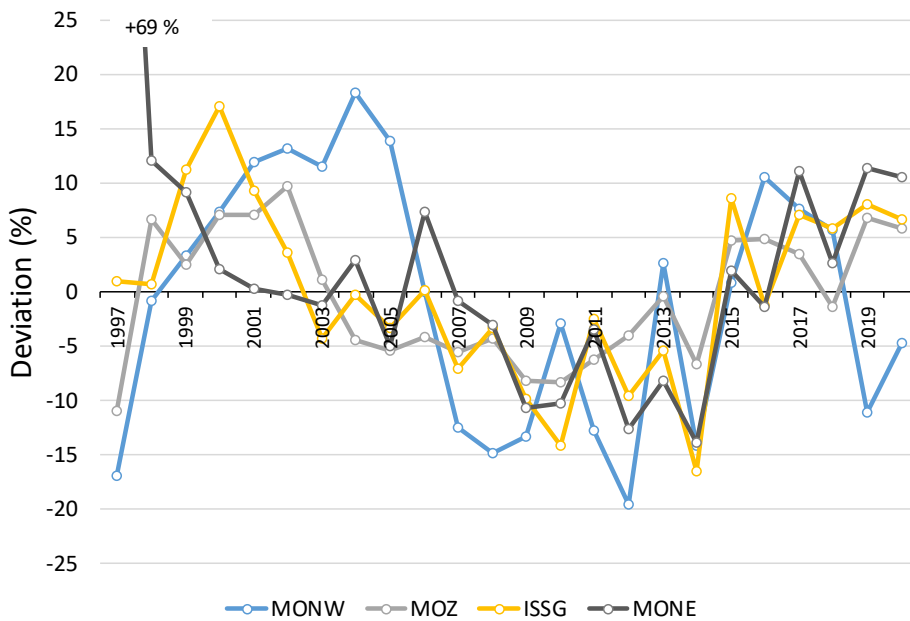


Fig. 9 – Deviation (in %) to the mean multi-annual SSC by large ecoregion

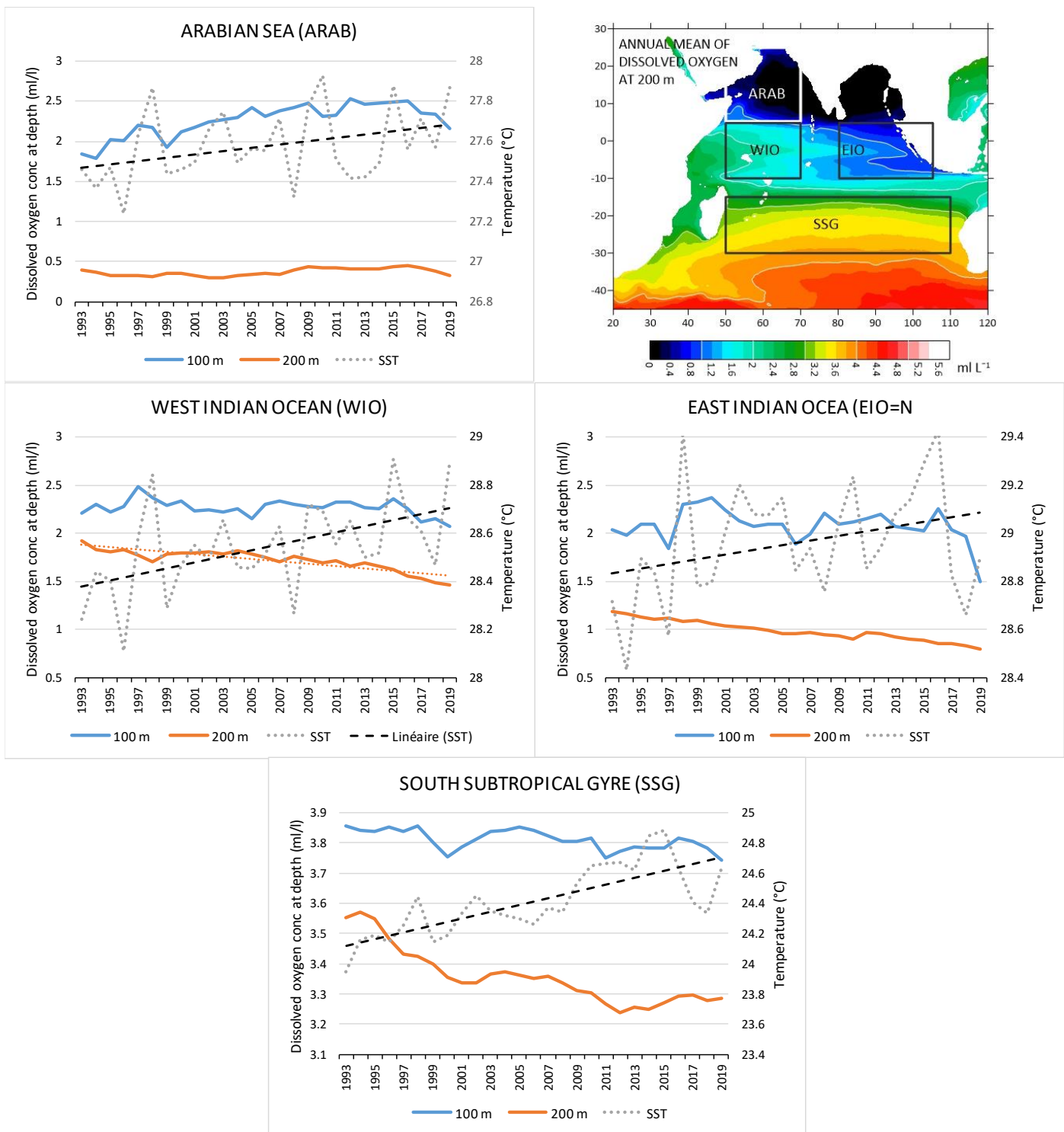


Fig. 10 – Trends in dissolved oxygen at 100 and 200 m depth (in ml/l) and sea surface temperature (SST, °C) in four large regions of the Indian Ocean: Arabian Sea (50E-70E / 5N-25N), West Indian Ocean (50E-70E / 10S-5N), East Indian Ocean (80E-105E / 10S-5N) and Indian South Subtropical Gyre (50E-110E / 30S-15S). The area boxes are overlaid on the mean annual DOC at 200 m, in the upper right panel, Source: CMEMS, *product code: global_reanalysis_bio_001_029*.